mathematics

MDPI

Article

Faulty Feeder Detection Based on Multiple Transient Characteristics Fusion in Resonant Grounding Systems

Ruihao Ma * and Qingle Pang

School of Information and Control Engineering, Qingdao University of Technology, Qingdao 266520, China; pangqingle@qut.edu.cn

* Correspondence: exmario5@163.com; Tel.: +86-197-0773-2582

Abstract

To address the low accuracy of faulty feeder detection methods based on single-fault characteristics, we propose a faulty feeder detection method for resonant grounding systems that fuses multiple transient characteristics. First, we analyze the transient zero-sequence current fault characteristics of both faulty and healthy feeders during single-phase-to-ground (SPG) faults. Then, the transient zero-sequence current of each feeder is decomposed into intrinsic mode functions (IMFs) using variational mode decomposition (VMD), and a new signal was constructed by combining IMF1 and IMF2. Subsequently, transient energy and waveform similarity fault characteristics are extracted from the constructed signal, and a faulty feeder detection criterion based on multiple transient characteristics fusion is developed. Finally, extensive simulations and field data verify the proposed faulty feeder detection method. The results demonstrate that the method is robust against fault resistance, fault inception angle, fault location, and noise, achieving high accuracy in faulty feeder detection. This method can be widely applied to detect faulty feeders in resonant grounding systems.

Keywords: resonant grounding system; single-phase-to-ground; faulty feeder detection; variational mode decomposition; transient energy; waveform similarity

MSC: 94C12; 94C05; 49M27

1. Introduction

With the continuous advancement of distribution automation, the demand for high power supply reliability in distribution networks is increasing. Distribution networks in China, Japan, and many European countries commonly employ the neutral non-effective grounding method [1]. Due to the weak grounding fault current during single-phase-to-ground (SPG) faults, detecting the faulty feeder in such systems is challenging, especially in resonant grounding systems [2,3]. SPG faults account for approximately 80% of faults in distribution networks [4,5], and if the faulty feeder is not accurately identified and promptly isolated, these faults can lead to severe consequences such as phase-to-phase short circuits and fire hazards [6]. Therefore, developing a highly accurate and reliable method for detecting SPG faulty feeders is crucial to ensuring power supply reliability in distribution networks.

In recent years, numerous faulty feeder detection techniques have emerged, primarily categorized into feature-analysis-based methods [1,3,7–21] and artificial-intelligence-based methods [4–6,22–28]. Feature-analysis-based methods are further divided into steady-state

Check for updates

Academic Editor: Zhanybai T. Zhusubaliyev

Received: 11 March 2026
Revised: 12 April 2026
Accepted: 18 April 2026
Published: 21 April 2026

Copyright: © 2026 by the authors. Licensee MDPI, Basel, Switzerland. This article is an open access article distributed under the terms and conditions of the Creative Commons Attribution (CC BY) license.

methods [1,7–10] and transient methods [3,11–21]. Steady-state methods based on fundamental waves are not applicable to resonant grounding systems, and the fault detection accuracy of steady-state methods based on harmonics is easily affected by the type of fault. Consequently, steady-state methods are rarely used in practical resonant grounding systems. Artificial-intelligence-based methods utilize advanced technologies such as deep learning [22,25], image processing [4,6], and particle swarm optimization algorithms [23] to detect faulty feeders by integrating multiple fault characteristics. Although very powerful, these techniques require faulty data samples that are representative of any fault scenarios, and their generalization capabilities are limited. To overcome these challenges, several advanced artificial intelligence methods for fault diagnosis have been proposed, including spatial-channel collaborative multi-scale graph interaction deep transfer learning [26], graph-guided multi-source interaction domain adaptation network [27], deep recurrent graph convolutional architecture [28], and non-linear directional residual versus machine-learning-based methods [29]. While these algorithms perform well on high-performance computers, the CPUs in faulty feeder detection devices are typically digital signal processors (DSPs) or microcontrollers, which have limited capacity for complex computations. Consequently, these methods are difficult to implement in practical field applications.

Transient methods utilize advanced modern signal processing techniques, such as the fast Fourier transform (FFT) [9,11], wavelet transform [12,13], Hilbert–Huang transform [5,14], empirical mode decomposition (EMD) [15], and variational mode decomposition (VMD) [17,18], to decompose transient zero-sequence current signals, extract fault characteristics (e.g., transient amplitude, energy, or polarity), and achieve faulty feeder detection. Due to the large amplitude and distinct characteristics of transient zero-sequence currents compared to steady-state zero-sequence currents, transient methods have become a prominent research focus. In [3], transient currents excluding fundamental frequency components were used to generate two fault indicators: transient energy within the first half power cycle and cosine similarity after the first half power cycle. The faulty feeder was identified based on the cumulative density function calculated from these two fault indicators. In [11], FFT was applied to calculate the fundamental components (FC), and faulty feeder detection was performed by obtaining transient zero-sequence current signals through subtracting the FC. However, these methods struggle to achieve accurate faulty feeder detection when transient zero-sequence currents are severely affected by noise interference. In [12], Flavio et al. presented a wavelet coefficient energy-based analysis for real-time fault-induced transient detection. In [13], Gao et al. utilized the empirical wavelet transform (EWT) to decompose differential faulty energy and adaptively selected the feature component with the largest permutation entropy. They employed a permutation variance index, constructed based on the sample point number and feature component energy, to detect high-impedance faults. Nevertheless, the accuracy of faulty feeder detection methods based on wavelet transform depends heavily on the choice of the mother wavelet function. In [14], Guo et al. used the Hilbert–Huang transform to decompose currents of all feeders connected to the bus into intrinsic mode functions (IMFs), detecting the faulty feeder by comparing the instantaneous amplitude of the first IMF. In [15], Wang et al. proposed a faulty feeder detection algorithm combining complete ensemble empirical mode decomposition with adaptive noise and Hilbert transform to construct a multi-criteria comprehensive voting method. However, the accuracy of these faulty feeder detection methods is susceptible to mode mixing and end effects.

To overcome the limitations of the aforementioned transient methods, the variational mode decomposition (VMD) algorithm has been applied to faulty feeder detection. In [17], Wang et al. proposed a high-impedance faulty feeder detection method that combined VMD with the Teager–Kaiser energy operator algorithm, utilizing VMD to extract the high-

frequency components of transient zero-sequence currents. In [18], Wang et al. employed VMD to eliminate interference from high-frequency components and extracted the low-frequency characteristic modes of the transient zero-sequence current of each feeder to detect faults. However, neither of these methods fully exploits the characteristics of both the high-frequency and low-frequency components of transient zero-sequence currents. To address this limitation, this paper proposes a faulty feeder detection method based on multiple transient characteristics fusion.

We propose a faulty feeder detection method based on the transient energy and waveform similarity of transient zero-sequence currents. The main contributions are as follows:

- We utilize VMD to decompose the transient zero-sequence current signals, remove the highest-frequency IMF, and then reconstruct a new transient zero-sequence current signal using the remaining IMFs. Subsequently, we calculate the transient energy of the reconstructed zero-sequence current signal.
- We select the three feeders with the largest transient energy, calculate their waveform similarities individually, and develop a faulty feeder detection criterion based on transient waveform similarity.
- We verify the proposed faulty feeder detection method using both simulation data and field fault current data. The results demonstrate that the method can reliably and accurately identify the faulty feeder.

2. Fault Characteristics Analysis of Transient Zero-Sequence Currents

Based on the third-order equivalent circuit of SPG faults in resonant grounding systems established in [20], the equivalent circuit of the resonant grounding system when feeder n experiences an SPG fault is shown in Figure 1 [3,21]. u_f (t) represents the equivalent virtual voltage source, it has the same magnitude but opposite phase relative to the pre-fault phase-to-ground voltage at the fault point. R denotes the equivalent resistance, which is the sum of the line-mode resistance, zero-mode resistance upstream of the fault point on the faulty feeder, and three times the fault resistance. L denotes the equivalent inductance, which is the sum of the line-mode inductance and zero-mode inductance upstream of the fault point on the faulty feeder. L_p represents the zero-sequence equivalent inductance of the Petersen coil, equal to three times the Petersen coil inductance. C_{0j} denotes the zero-sequence distributed capacitance to ground of feeder j (j = 1, 2, . . ., n). I_{0f} is zero-sequence current at the fault point. I_{0j} represents the zero-sequence current of feeder j (j = 1, 2, . . ., n). I_{0Cn} is the zero-sequence distributed capacitance current to ground of the faulty feeder n. i_{Lp} is the current through the Petersen coil.

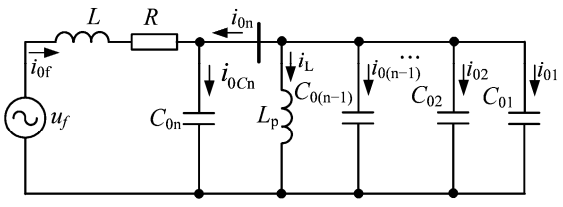


Figure 1. Zero-sequence equivalent circuit under SPG faults.

When a low-impedance grounding fault occurs, the inductive reactance of the Petersen coil is much greater than the capacitive reactance of the capacitors; therefore, the impact

of the Petersen coil on the transient zero-sequence current can be neglected [3,21]. The zero-sequence current i_{0n} in the faulty feeder n can be calculated as follows [3]:

$$\begin{cases} i_{0n} = i_{0n_\mathrm{FFC}} + i_{0n_\mathrm{TC}} \\ i_{0n_\mathrm{FFC}} = -U_\mathrm{m}\omega_0(C_{0\Sigma} - C_{0n})\cos(\omega_0 t + \varphi) \\ i_{0n_\mathrm{TC}} = -U_\mathrm{m}\omega_0(C_{0\Sigma} - C_{0n})[(A_1 \sin\varphi \sin\omega_\mathrm{f} t - \cos\varphi \sin\omega_\mathrm{f} t)\mathrm{e}^{-\delta t} \end{cases}, \quad (1)$$

where i_{0n_FFC} and i_{0n_TC} are the fundamental frequency components (FFCs) and transient components (TCs) of i_{0n}, respectively; U_m is the peak value of u_f; $C_{0\Sigma}$ is the sum of zero-sequence distributed capacitances to ground of all feeders; ω_0 is the fundamental angular frequency; φ is the fault inception angle; δ is the damping ratio, defined as $\delta = R_\mathrm{f}/(2L)$; and ω_f is the resonant angular frequency of the transient process, defined as $\omega_\mathrm{f} = \sqrt{1/(LC_{0\Sigma}) - (R_f/(2L))^2}$, $A_1 = 1/(\omega_0\omega_\mathrm{f}LC_{0\Sigma})\sin\varphi + \delta/\omega_\mathrm{f}\cos\varphi$.

The zero-sequence current i_{0j} in the healthy feeder j can be calculated as follows [3,21]:

$$\begin{cases} i_{0j} = i_{0j_\mathrm{FFC}} + i_{0j_\mathrm{TC}} \\ i_{0j_\mathrm{FFC}} = U_\mathrm{m}\omega_0 C_{0j}\cos(\omega_0 + \varphi) \\ i_{0j_\mathrm{TC}} = U_\mathrm{m}\omega_0 C_{0j}[(A_1 \sin\varphi \sin\omega_\mathrm{f} t - \cos\varphi \sin\omega_\mathrm{f} t)\mathrm{e}^{-\delta t} \end{cases}. \quad (2)$$

From Equations (1) and (2), i_{0n} and i_{0k} consist of two components: one is the FFCs, the other is the TCs. The direction of the TCs of the transient zero-sequence current in the faulty feeder is opposite to that in the healthy feeder. Moreover, the amplitude of the TCs in the faulty feeder is relatively large and significantly greater than that in the healthy feeder. In contrast, the FFCs of the transient zero-sequence current in the faulty feeder are similar to those in the healthy feeder. Therefore, faulty feeder detection can be effectively achieved by extracting the TCs.

When the grounding fault resistance R_f is high, L_p cannot be neglected, whereas L can be disregarded. If $R_\mathrm{f} > 0.5\sqrt{L_\mathrm{p}/C_{0\Sigma}}$, the system is in an underdamping state. The zero-sequence current i_{0n} in the faulty feeder n can be calculated as follows [3,21]:

$$\begin{cases} i_{0n} = i_{0n_\mathrm{FFC}} + i_{0n_\mathrm{TC}} \\ i_{0n_\mathrm{FFC}} = [\omega_0^2 L_\mathrm{p}(C_{0\Sigma} - C_{0n}) - 1]A\sin(\omega_0 t + \theta) \\ i_{0n_\mathrm{TC}} = -[B_1 + L_\mathrm{p}(C_{0\Sigma} - C_{0n})(B_1\delta^2 - B_1\omega_\mathrm{f}^2 - 2B_2\omega_\mathrm{f}\delta)]\cos\omega_\mathrm{f} t\mathrm{e}^{-\delta t} \\ \qquad -(B_2 + L_\mathrm{p}(C_{0\Sigma} - C_{0n})(B_2\delta^2 - B_2\omega_\mathrm{f}^2 + 2B_1\omega_\mathrm{f}\delta)]\sin\omega_\mathrm{f} t\mathrm{e}^{-\delta t} \end{cases}, \quad (3)$$

where $A = U_m/\sqrt{R_\mathrm{f}^2 + \omega_0^2 L_\mathrm{p}^2/(1 - \omega_0^2 L_\mathrm{p} C_{0\Sigma})^2}$; $B_1 = -A\sin\theta$; $B_2 = -(\delta A\sin\theta + \omega_0 A\cos\theta)/\omega_\mathrm{f}$; $\delta = 1/(2R_\mathrm{f}C_{0\Sigma})$; $\omega_\mathrm{f} = \sqrt{1/(LC_{0\Sigma}) - [1/(2R_\mathrm{f}C_{0\Sigma})]^2}$; and $\theta = \varphi - \arctan\{\omega_0 L_\mathrm{p}/[R(1 - \omega_0^2 L_\mathrm{p} C_{0\Sigma})]\}$.

The zero-sequence current i_{0j} in the healthy feeder j can be calculated as follows [3,21]:

$$\begin{cases} i_{0j} = i_{0j_\mathrm{FFC}} + i_{0j_\mathrm{TC}} \\ i_{0j_\mathrm{FFC}} = -\omega_0^2 L_\mathrm{p} C_{0j} A\sin(\omega_0 t + \theta) \\ i_{0j_\mathrm{TC}} = L_\mathrm{p} C_{0j}(B_1\delta^2 - B_1\omega_\mathrm{f}^2 - 2B_2\omega_\mathrm{f}\delta)]\cos\omega_\mathrm{f} t\mathrm{e}^{-\delta t} \\ \qquad +L_\mathrm{p} C_{0j}(B_2\delta^2 - B_2\omega_\mathrm{f}^2 + 2B_1\omega_\mathrm{f}\delta)]\sin\omega_\mathrm{f} t\mathrm{e}^{-\delta t} \end{cases}. \quad (4)$$

If $R_\mathrm{f} < 0.5\sqrt{L_\mathrm{p}/C_{0\Sigma}}$, the system is in an overdamping state. The zero-sequence current i_{0n} in the faulty feeder n can be calculated as follows [21]:

$$\begin{cases} i_{0n} = i_{0n_\mathrm{FFC}} + i_{0n_\mathrm{TC}} \\ i_{0n_\mathrm{FFC}} = [\omega_0^2 L_\mathrm{p}(C_{0\Sigma} - C_{0n}) - 1]B\sin(\omega_0 t + \theta) \\ i_{0n_\mathrm{TC}} = (\frac{L_\mathrm{p} p_1 D_1}{R} + L_\mathrm{p} C_{0n} D_1 p_1^2)\mathrm{e}^{p_1 t} + (\frac{L_\mathrm{p} p_2 D_2}{R} + L_\mathrm{p} C_{0n} D_2 p_2^2)\mathrm{e}^{p_2 t} \end{cases}, \quad (5)$$

where $B = U_m/[|Z|(1-\omega_0^2 L_p C_{0\Sigma})]$; $Z = R + j\omega_0 L_p/(1-\omega_0^2 L_p C_{0\Sigma})$; $D_1 = (\omega_0 B\cos\theta - p_2 B\sin\theta)/(p_2-p_1)$; $D_2 = -(\omega_0 B\cos\theta - p_1 B\sin\theta)/(p_2-p_1)$; $p_1 = -1/(2RC_{0\Sigma}) - \sqrt{1/(2RC_{0\Sigma})^2 - 1/(L_p C_{0\Sigma})}$; and $p_2 = -1/(2RC_{0\Sigma}) + \sqrt{1/(2RC_{0\Sigma})^2 - 1/(L_p C_{0\Sigma})}$.

The zero-sequence current i_{0j} in the healthy feeder j can be calculated as follows [21]:

$$\begin{cases} i_{0j} = i_{0j_FFC} + i_{0j_TC} \\ i_{0j_FFC} = -\omega_0^2 L_p C_{0j} B\sin(\omega_0 t + \theta) \\ i_{0j_TC} = L_p C_{0j}(D_1 p_1^2 e^{p_1 t} + D_2 p_2^2 e^{p_2 t}) \end{cases}. \quad (6)$$

From Equations (3)–(6), the amplitudes and directions of the FFCs in both the faulty and healthy feeders are nearly identical. The amplitude of the TCs in the faulty feeder is slightly greater than that in the healthy feeder. Therefore, detecting the faulty feeder during high-impedance faults (HIFs) is very challenging.

As the Petersen coil is a dynamic component, its inductive current undergoes a transient process before reaching a steady-state value following an SPG fault. At the initial stage of SPG faults, the inductive current of the Petersen coil is very small, causing the coil to behave like a large inductance. According to Equations (5) and (6), the amplitude of the FFCs in the faulty feeder is greater than that in the healthy feeders, and the direction of the FFCs in the faulty feeder is opposite to that in the healthy feeders during the initial stage of SPG faults. Therefore, faulty feeder detection can be achieved by extracting FFCs or TCs for any SPG faults.

3. Faulty Feeder Detection Criterion

3.1. Signal Decomposition Based on VMD

To achieve faulty feeder detection, it is first necessary to obtain the FFCs and TCs of transient zero-sequence current signals. Since the resonant frequency of TCs varies with different fault types and transient zero-sequence currents are susceptible to external interference, such as measurement errors, noise, and harmonic pollution, adaptive and non-recursive signal decomposition techniques must be employed. VMD is a recently developed multi-resolution technique for adaptive and non-recursive signal decomposition [30]. It iteratively decomposes the input signal to obtain K IMFs, making it highly suitable for faulty feeder detection based on transient zero-sequence currents.

The larger the parameter K in VMD, the greater the computational complexity and the longer the runtime. To effectively extract low-frequency and transient components from transient zero-sequence currents, it is preferable to keep the parameter K as small as possible. Therefore, we set K to 3. Using VMD, the transient zero-sequence current of each feeder is decomposed into IMF_1, IMF_2, and IMF_3. Among these, IMF_1 represents the low-frequency components, including the FFCs; IMF2 captures the high-frequency components, primarily the TCs; and IMF3 corresponds to interference and residual components. Therefore, IMF1 and IMF2 are selected as the characteristic IMFs, and the following signal is reconstructed:

$$i_{cj} = u_{1j} + u_{2j}, \quad (7)$$

where i_{cj} is the reconstructed signal of the j-th feeder; u_{j1} and u_{j2} is the expressions for IMF_1 and IMF_2 of the j-th feeder, respectively. The reconstructed signal contains both the FFCs and the TCs, while eliminating interference signals, and can be used for faulty feeder detection.

Due to the distinct fault characteristics of the transient zero-sequence current signal in the faulty feeder during the initial stage of SPG faults, the data window for transient zero-sequence currents used in faulty feeder detection is selected as the first quarter of the power cycle.

3.2. Transient Energy-Based Faulty Feeder Detection Criterion

The waveforms of the IMF_k generated by different types of grounding faults vary significantly, making it challenging to calculate the amplitude of the reconstructed signal i_{cj} directly. Therefore, the transient energy of the reconstructed signal i_{cj} during the first quarter of the power cycle after SPG faults is used to represent its amplitude.

$$E_j = \sum_{m=1}^{M} i_{cj}^2(m), \tag{8}$$

where E_j represents the transient energy of the j-th feeder; m denotes the index of the sampling point; M signifies the total number of sampling points within a quarter power cycle; $i_{cj}(m)$ indicates the m-th sampled value of the reconstructed signal i_{cj}.

The proportion of transient energy contributed by each feeder to the total transient energy of all feeders connected to the bus varies. The transient energy proportion is calculated as follows:

$$\begin{cases} \Delta_j = \frac{E_j}{E_\Sigma} \\ E_\Sigma = \sum_{j=1}^{n} E_j \end{cases}, \tag{9}$$

where Δ_j represents the transient energy proportion of the j-th feeder; E_Σ denotes the total energy of all feeders connected to the bus; and n signifies the total number of feeders.

The amplitude of the transient zero-sequence current in the faulty feeder equals the sum of the amplitudes of the transient zero-sequence currents in the healthy feeders; however its direction is opposite. That is,

$$i_j = -\sum_{k=1,k\neq j}^{n} i_k, \tag{10}$$

where i_j represents the transient zero-sequence current in the faulty feeder, and i_k denotes the transient zero-sequence current in the j-th healthy feeder. Therefore, the transient energy proportion of the faulty feeder satisfies $\Delta_j > 0.5$ and increases as the number of feeders grows.

The faulty feeder detection criterion based on transient energy is as follows: if the transient energy proportion of the j-th feeder satisfies the following inequality, then feeder j is identified as the faulty; otherwise, it is considered healthy.

$$\Delta_j > \Delta_{th}, \tag{11}$$

where Δ_{th} represents the threshold for faulty feeder detection criteria. If the reliability coefficient is set between 1 and 1.6, then the range of Δ_{th} is 0.5 to 0.8. The value of Δt_h increases as the number of feeders increases.

3.3. Waveform-Similarity-Based Faulty Feeder Detection Criterion

At the initial stage of SPG faults, there is a significant difference in the transient zero-sequence current waveforms between the faulty feeder and the healthy feeders, while the transient zero-sequence current waveforms of the healthy feeders remain similar. Therefore, faulty feeder detection can be achieved by comparing the waveform similarity of the

reconstructed transient zero-sequence current signals during the first quarter of a power cycle following an SPG fault. The waveform similarity is calculated as follows:

$$\rho_{jk} = \frac{\sum_{m=1}^{M} i_{cj}(m) i_{ck}(m)}{\sqrt{\sum_{m=1}^{M} i_{cj}^2(m) i_{ck}^2(m)}}, \tag{12}$$

where ρ_{jk} represents the waveform similarity between the transient zero-sequence currents of the j-th and k-th feeders; $i_{cj}(m)$ and $i_{ck}(m)$ are the m-th sampled values of the reconstructed signal i_{cj} and i_{ck}, respectively.

To detect the faulty feeder, the waveform similarity coefficient ρ_j of the transient zero-sequence current of the j-th feeder is calculated as follows:

$$\rho_j = \begin{cases} \max\limits_{k=1,k\neq j}^{n} \rho_{jk}, & \exists \rho_{jk} > 0 \\ \min\limits_{k=1,k\neq j}^{n} \rho_{jk}, & \text{others} \end{cases}. \tag{13}$$

The proportion η_j of the waveform similarity coefficient for the j-th feeder relative to the total similarity coefficient of all feeders is calculated as follows:

$$\begin{cases} \eta_j = \frac{\rho_j}{\rho_\Sigma} \\ \rho_\Sigma = \sum\limits_{j=1}^{n} |\rho_j| \end{cases}, \tag{14}$$

where η_j represents the proportion of the waveform similarity coefficient for the j-th feeder, and ρ_Σ denotes the sum of the waveform similarity coefficients for all feeders connected to the bus.

The number of feeders in a typical distribution network generally ranges from three to ten. The range of ρ_j for faulty feeders is between -1 and -0.3, while for healthy feeders, it ranges from 0.3 to 1. Therefore, in a distribution network with three feeders, the range of η_j for faulty feeders is from -0.63 to -0.13, whereas for healthy feeders, it is from 0.19 to 0.44. In a network with ten feeders, the range of η_j for faulty feeders is from -0.27 to -0.03, and for healthy feeders, it is from 0.03 to 0.23. Overall, in a typical distribution network, the range of η_j for faulty feeders spans from -0.63 to -0.03, while for healthy feeders, it ranges from 0.03 to 0.44.

The faulty feeder detection criterion based on waveform similarity is as follows: if the waveform similarity coefficient proportion η_j of the transient zero-sequence current in the j-th feeder satisfies the following inequality, then feeder j is identified as the faulty; otherwise, it is considered healthy.

$$\eta_j < \eta_{\text{th}}, \tag{15}$$

where η_{th} represents the threshold value for the faulty feeder detection criterion, the range of η_{th} is set from -0.2 to -0.05 considering the reliability of faulty feeder detection. η_{th} takes a larger value when the number of feeders is large and a smaller value when the number of feeders is small. If all feeders fail to meet the faulty feeder detection criteria, the fault is determined to be a bus fault.

3.4. Fusion-Based Faulty Feeder Detection Criterion

In various SPG fault scenarios in distribution networks, the amplitude or waveform characteristics of transient zero-sequence currents in the faulty feeder may not be distinctly evident. Consequently, the accuracy of faulty feeder detection based on a single fault char-

acteristic tends to be relatively low. To improve detection accuracy, this paper proposes a faulty feeder detection method for resonant grounding systems based on multiple transient characteristics fusion, which integrates the amplitude and waveform characteristics of transient zero-sequence currents.

The faulty feeder detection method based on transient energy is less affected by interference and provides higher accuracy. However, in cases involving long feeders or HIFs, multiple feeders may exhibit large transient energy proportion, making it difficult to accurately identify the faulty feeder. Additionally, when the transient zero-sequence current of a feeder is small, interference can cause a large waveform similarity error, leading to incorrect detection results using the waveform similarity-based method. To address these challenges, a fusion-based faulty feeder detection criterion has been developed: first, calculate the transient energy of the reconstructed signals for the transient zero-sequence currents of all feeders; then, select the three feeders with the highest transient energy. The waveform similarity comparison method is applied to these three feeders to identify the faulty feeder. If none of the feeders meet the detection criteria, the fault is determined to be a bus fault.

3.5. Procedure of Fusion-Based Faulty Feeder Detection

The proposed faulty feeder detection method is implemented only when an SPG fault occurs. An SPG fault event is identified when the measured zero-sequence voltage U_0 meets the following conditions:

$$U_0 > kU_N, \tag{16}$$

where U_N represents the rated phase voltage, and k denotes the reliability factor, which is typically set at 15%.

The flowchart of the proposed fusion-based faulty feeder detection algorithm is shown in Figure 2. The steps of the algorithm are as follows:

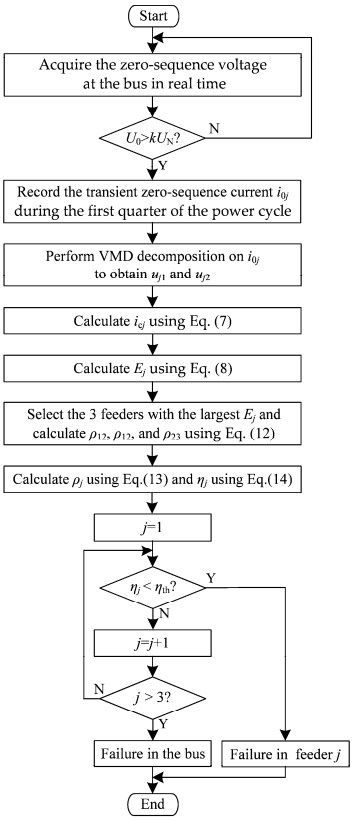


Figure 2. Flow chart of fusion-based faulty feeder detection algorithm.

Step 1: Acquire the zero-sequence voltage at the bus in real time and calculate U_0.

Step 2: If $U_0 > kU_N$ is satisfied, start the faulty feeder detection algorithm.

Step 3: Record the transient zero-sequence current signal i_{0j} in each feeder during the first quarter of the power cycle.

Step 4: Perform VMD on i_{0j} to obtain u_{j1} and u_{j2}.

Step 5: Calculate the reconstructed signal i_{cj} using Equation (7).

Step 6: Calculate E_j using Equation (8).

Step 7: Select the three feeders with the largest transient energy and calculate ρ_{12}, ρ_{13}, and ρ_{23} using Equation (12), respectively.

Step 8: Calculate ρ_j using Equation (13) and η_j using Equation (14).

Step 9: If η_j satisfies Inequality (15), feeder j is identified as the faulty feeder; otherwise, it is considered healthy. If none of the three feeders meet the faulty feeder detection criteria, the fault is determined to be a bus fault.

4. Simulation Analysis

4.1. Simulation Model

A typical radial distribution network model with four feeders has been developed in MATLAB R2021b, as shown in Figure 3. The lengths of the feeders are marked in the figure, and the parameters are listed in Table 1 [23]. In Figure 3, R_L and L_N represent the resistance and inductance of the Petersen coil connected to the Z-type grounding transformer. The overcompensation degree is 8%, R_L = 3 Ω, and L_N = 294.3 mH. The system sampling frequency is set to 10 kHz.

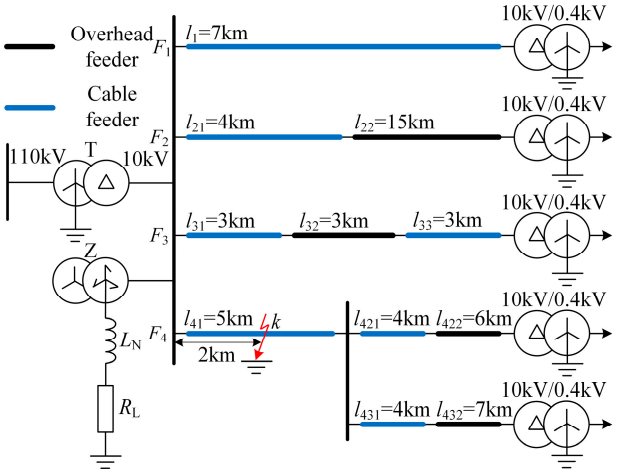


Figure 3. Simulation mode with four feeders.

Table 1. Feeder parameters.

Line Type	Phase Sequence	*R* (Ω/km)	*L* (mH/km)	*C* (μF/km)
Overhead line	Zero sequence	0.125	1.3	0.0096
	Positive sequence	0.275	4.6	0.0054
Cable line	Zero sequence	0.27	0.255	0.339
	Positive sequence	2.7	1.019	0.28

4.2. Verification of Extracted Fault Characteristics

To verify the fault characteristics extracted in Section 2, the simulation model shown in Figure 3 is used to analyze the following two types of SPG faults. A larger penalty factor in VMD may result in over-decomposition, while a smaller penalty factor can lead to mode

mixing [31]. To effectively extract the FFCs and TCs while suppressing noise, the penalty factor α is set to 20,000. The personal computer used in this study is equipped with an Intel® Core™ i7-10700 CPU running at 2.90 GHz, 16.0 GB of RAM, and a 64-bit Windows operating system. The MATLAB program implementing the faulty feeder detection algorithm has a runtime of approximately 0.061 s. These results satisfy the requirements for practical engineering applications. Certainly, porting this algorithm to DSP or FPGA platforms for faulty feeder detection devices will require optimizing the VMD computation and converting it to fixed-point arithmetic.

4.2.1. Case 1

An SPG fault occurs at point k on the fourth feeder (F_4), located 2 km from the bus, with a ground fault resistance R_g = 5 Ω, and a fault inception angles φ = 90°. The transient zero-sequence currents of F_4 are shown in Figure 4. The transient zero-sequence currents are decomposed using VMD, and the decomposed modal functions IMF_1, IMF_2, and IMF_3 are presented in Figure 4. It can be observed that there are significant differences in the amplitude and waveform of IMF_1 and IMF_2 between the faulty feeder and the healthy feeders. The FFCs included in IMF_1 are shown in Figure 5. As illustrated, there are notable differences between the FFCs of the faulty feeder and those of the healthy feeders during the initial stage of the SPG fault. Therefore, FFCs cannot be eliminated when using transient zero-sequence current for faulty feeder detection. The reconstructed signals using IMF_1 and IMF_2 for each feeder are shown in Figure 6. The figure demonstrates that there is a significant difference between the reconstructed signals of the faulty feeder and those of the healthy feeders under low impedance faults (LIFs), which can be used to reliably detect the faulty feeder.

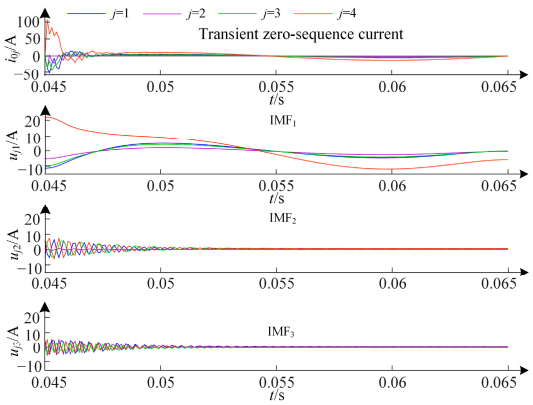


Figure 4. VMD results of transient zero-sequence currents in case 1.

4.2.2. Case 2

An SPG fault occurs at point k on F_4, located 2 km from the bus, with a ground fault resistance R_g = 2000 Ω and a fault inception angles φ = 90°. The transient zero-sequence currents of F_4 are shown in Figure 7. The decomposed modal functions IMF_1, IMF_2, and IMF_3 obtained using VMD are also presented in Figure 7. It can be observed that there are significant differences in the amplitude and waveform of IMF_1 between the faulty feeder and the healthy feeders. The FFCs included in IMF_1 are shown in Figure 8. As illustrated, there are notable differences between the FFCs of the faulty feeder and those of the healthy feeders during the initial stage of the fault. Therefore, FFCs cannot be disregarded when using transient zero-sequence current for faulty feeder detection. The reconstructed signals using IMF_1 and IMF_2 for each feeder are shown in Figure 9. The figure reveals a significant difference between the reconstructed signals of the faulty feeder and those of the healthy feeders under HIFs, which can be used to reliably detect the faulty feeder. Consequently,

whether the fault is an HIF or an LIF, the fault characteristics can be reliably extracted using the reconstructed signals.

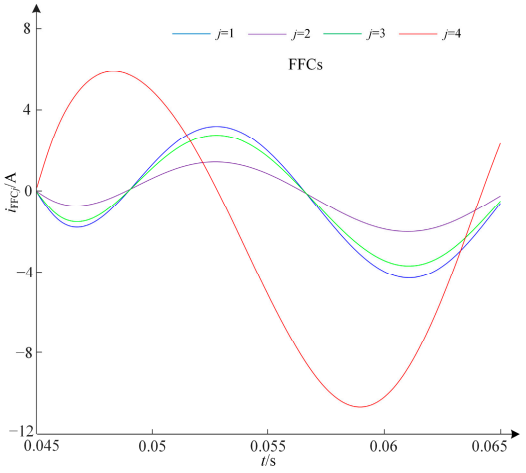


Figure 5. FFCs of transient zero-sequence currents in case 1.

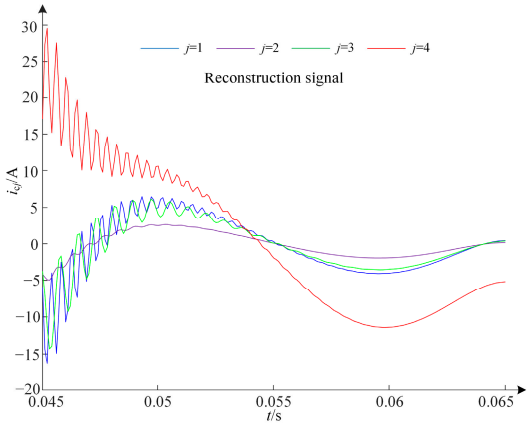


Figure 6. Reconstruction signals in case 1.

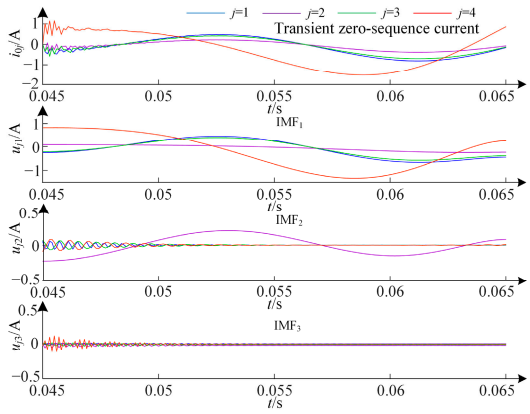


Figure 7. VMD results of transient zero-sequence currents in case 2.

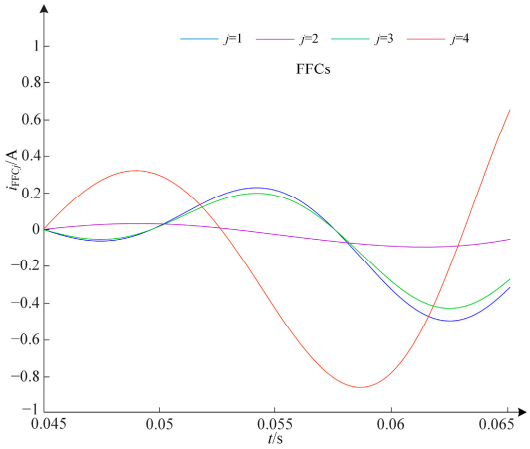


Figure 8. FFCs of transient zero-sequence currents in case 2.

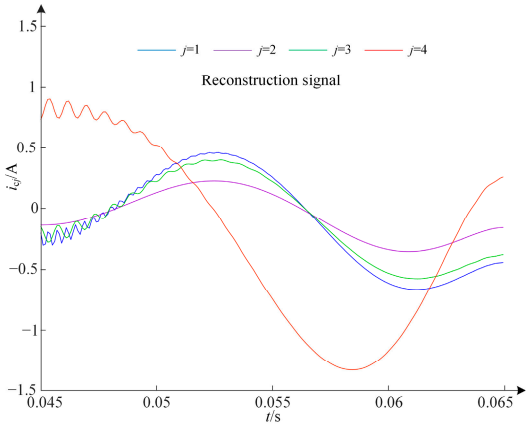


Figure 9. Reconstruction signals in case 2.

4.3. Verification of the Proposed Faulty Feeder Detection Method

Many SLG fault scenarios under various fault conditions are simulated. These scenarios include different fault phases (phase A, B, or C), fault locations (at the bus or at 10%, 40%, 70%, or 90% along feeders 1–4), fault inception angles (0°, 45°, 90°, or 135°), and fault resistances (1 Ω, 10 Ω, 100 Ω, 1000 Ω, 2000 Ω, 3000 Ω, 4000 Ω, or 5000 Ω). In the 1632 fault scenarios, the proposed faulty feeder detection method can reliably identify all faulted feeders or the faulty bus.

Several partial simulation data and faulty feeder detection results are presented in Table 2. Here, F_j represents the serial number of the faulty feeder, φ denotes the fault inception angle, R_g stands for the fault resistance, E_j signifies the transient energy, ρ_j indicates the waveform similarity coefficient, and η_j represents the waveform similarity coefficient proportion. By setting the threshold η_{th} to −0.1, all faulty feeder detection results are correct. Therefore, the proposed method can accurately detect the faulty feeder, and its reliability is not affected by fault conditions.

Table 2. Simulation data of distribution network with four feeders.

Cases	F_j	Position	φ (°)	R_g (Ω)	E_j	ρ_j	η_j	Results
1	2	90%	0	1	894, 22,713, 673, 2051	0.9408, −0.9743, 0.9408	0.3294, −0.3412, 0.3294	Feeder 2
2	2	90%	45	1	1362, 29,367, 1639, 5627	−0.8768, 0.9439, 0.9439	−0.3171, 0.3414, 0.3414	Feeder 2
3	2	90%	90	10	1907, 22,984, 1492, 9812	0.9929, −0.9034, 0.9929	0.3437, −0.3127, 0.3437	Feeder 2

Table 2. *Cont.*

Cases	F_j	Position	φ (°)	R_g (Ω)	E_j	ρ_j	η_j	Results
4	2	90%	90	1000	5.1162, 132.7223, 4.2172, 19.239	0.8466, −0.6390, 0.8466	0.3630, −0.2740, 0.3630	Feeder 2
5	4	10%	0	2000	1.3112, 0.2898, 0.9835, 16.9661	1, 1, −0.9688	0.3368, 0.3368, −0.3263	Feeder 4
6	4	10%	45	100	297, 62.1, 224.12, 5190.3	0.9756, 0.9756, −0.6334	0.3775, 0.3775, −0.2451	Feeder 4
7	4	10%	45	3000	0.8764, 0.2035, 0.6637, 20.3033	0.9915, 0.9915, −0.7338	0.3649, 0.3649, −0.2701	Feeder 4
8	4	10%	90	3000	0.6884, 0.1935, 0.5229, 12.9077	0.9659, 0.9659, −0.4179	0.4111, 0.4111, −0.1779	Feeder 4
9	Bus	–	45	10	1050.2, 166.5, 883.9, 4175.1	0.8968, 0.9260, 0.9260	0.3262, 0.3369, 0.3369	bus
10	Bus	–	90	100	346, 67, 277, 1297.3	0.9659, 0.9770, 0.9770	0.3308, 0.3346, 0.33465	bus

4.4. Noise Interference Test

White noise signals with signal-to-noise ratios (SNR) of 5 dB, 10 dB, and 20 dB are added to the transient zero-sequence currents in the fault scenarios described in Section 4.3 to verify the anti-interference capability of the proposed faulty feeder detection method. Figure 10 shows the zero-sequence currents and IMFs when an SPG occurs at 10% of F_4 with a fault inception angle of 0°, a fault resistance of 1000 Ω, and an SNR of 5 dB. From the figure, it is evident that the transient zero-sequence current signals are severely affected by strong noise, making it difficult to distinguish the faulty feeder from the healthy feeder based solely on the noisy zero-sequence current signals. However, after applying VMD to the transient zero-sequence currents, the fault characteristics in IMF1 and IMF_2 become apparent, enabling accurate detection of the faulty feeder. Partial simulation data with noise and the corresponding faulty feeder detection results are presented in Table 3. As shown, the proposed faulty feeder detection method is robust against noise and can accurately identify faulty feeders.

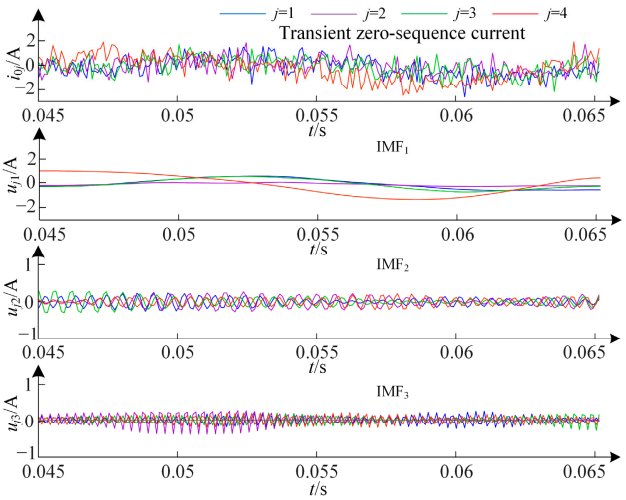


Figure 10. Transient zero-sequence currents with the noise (SNR = 5 dB) and IMFs.

Table 3. Simulation results under noise interference.

Cases	F_i	Position	φ (°)	R_g (Ω)	*SNR*	E_j	η_j	Results
1	2	90%	45	100	5	249.4, 6173.4, 197.3, 863.7	0.3553, −0.2894, 0.3553	Feeder 2
2	2	90%	45	100	10	248.5, 6223.3, 192, 885.2	0.3563, −0.2874, 0.3563	Feeder 2
3	2	90%	45	100	20	238.9, 6323.3, 190.2, 935.7	0.3544, −0.2911, 0.3544	Feeder 2
4	4	10%	90	2000	5	3.4377, 1.1145, 2.1192, 29.1335	0.2902, 0.2902, −0.4197	Feeder 4
5	4	10%	90	2000	10	1.9031, 0.4352, 1.4652, 25.1508	0.3927, 0.3927, −0.2146	Feeder 4
6	4	10%	90	2000	20	1.2807, 0.3594, 1.1829, 28.0953	0.4142, 0.4142, −0.1716	Feeder 4
7	Bus	–	0	10	5	544.2, 121.9, 408.1, 1997.4	0.3333, 0.3333, 0.3333	Bus
8	Bus	–	0	10	10	542.5, 126.5, 407.7, 1970.5	0.3332, 0.3334, 0.3334	Bus
9	Bus	–	0	10	20	545.5, 122.4, 414.5, 1955.6	0.3332, 0.3334, 0.3334	Bus

4.5. Detection Results Based on Different Fault Characteristics

To compare the discriminative power of the reconstructed signal with that of individual IMFs (IMF1 or IMF2), white noise signals with SNR of 10 dB are added to the transient zero-sequence currents in the fault scenarios described in Section 4.3 for simulation analysis. Table 4 summarizes the accuracy rates (AR), false positive rates (FPR), and false negative rates (FNR) of the faulty feeder detection methods based on reconstructed signals, IMF1, and IMF2, respectively. The table shows that the proposed method achieves a higher detection accuracy.

Table 4. Comparison of the faulty feeder detection methods based on different fault characteristics.

Fault Characteristics	FPR	FNR	AR
IMF1	3.7%	3.7%	96.3%
IMF2	25.0%	2.9%	75.0%
Reconstructed Signals	2.2%	2.2%	97.8%

4.6. Scalability Test

To evaluate the scalability of the proposed faulty feeder detection method, we develop a distribution network model with ten feeders in MATLAB, as shown in Figure 11. The lengths of the feeders are indicated in the figure, and the parameters are listed in Table 1. In Figure 11, QF represents a bus section breaker that remains closed during normal system operation. The overcompensation degree is 8%, $R_{L1} = R_{L2} = 3\ \Omega$, $L_{N1} = 406.1$ mH, and $L_{N2} = 488.6$ mH. The SPG faults are located 2 km from the busbar on feeders 1 to 10, the fault inception angles are 0°, 45°, or 90°, and the fault resistances are 1 Ω, 10 Ω, 100 Ω, 1000 Ω, 3000 Ω, or 5000 Ω. Across the 180 fault scenarios, the proposed faulty feeder detection method reliably identify all faulted feeders. Several partial simulation data and detection results are presented in Table 5, which confirms that all faulty feeder detections are accurate. Therefore, the proposed method is applicable to large-scale distribution networks and demonstrates strong scalability.

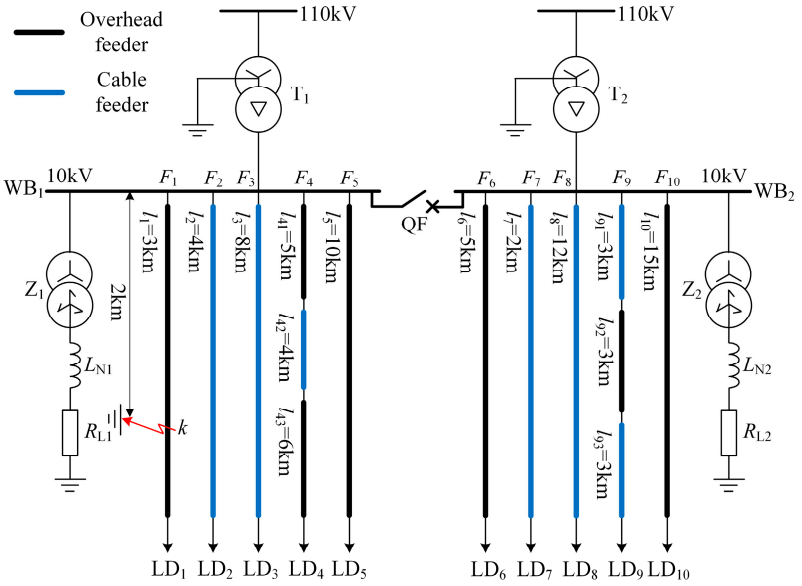


Figure 11. Simulation mode with ten feeders.

Table 5. Simulation data of distribution network with ten feeders.

Cases	F_j	φ (°)	R_g (Ω)	E_j	ρ_j	η_j	Results
1	1	0	10	36,798, 181, 611, 1411, 0.4, 1, 417, 1364, 39, 0.1	−0.9025, 0.9275, 0.9275	−0.3273, 0.33364, 0.3364	Feeder 1
2	1	45	10	57,212, 334, 1357, 2946, 0.8, 1, 800, 3069, 82, 0.03	−0.8394, 0.9290, 0.9290	−0.3112, 0.3444, 0.3444	Feeder 1
3	1	90	10	67,250, 506, 2067, 4546, 1, 2, 1239, 4701, 121, 0.26	−0.8296, 0.9124, 0.9124	−0.3126, 0.3437, 0.3437	Feeder 1
4	1	0	1000	128.9, 0.768, 3.057, 5.893, 0.002, 0.004, 0.004, 1.76, 6.873, 0.193, 0.0005	−0.9881, 1.000, 1.000	−0.3307, 0.3347, 0.3347	Feeder 1
5	1	45	1000	258.97, 1.243, 4.635, 8.942, 0.003, 0.006, 2.715, 10.49, 0.272, 0.0005	−0.8613, 0.9856, 0.9856	−0.3041, 0.348, 0.348	Feeder 1
6	1	90	1000	182.8, 1.033, 3.563, 6.905, 0.002, 0.005, 2.136, 8.056, 0.2, 0.002	−0.7094, 0.9584, 0.9584	−0.2701, 0.3649, 0.3649	Feeder 1
7	1	0	3000	17.655, 0.092, 0.365, 0.703, 0.0002, 0.0005, 0.21, 0.82, 0.023, 0.0001	−0.9864, 1.000, 1.000	−0.3303, 0.3349, 0.3349	Feeder 1
8	1	45	3000	31.273, 0.159, 0.56, 1.073, 0.0003, 0.0008, 0.323, 1.246, 0.032, 0.0002	−0.8644, 0.9868, 0.9868	−0.3046, 0.3477, 0.3477	Feeder 1
9	1	90	3000	22.333, 0.143, 0.416, 0.754, 0.0002, 0.0007, 0.244, 0.919, 0.022, 0.0006	−0.7106, 0.9888, 0.9888	−0.2644, 0.3678, 0.3678	Feeder 1

4.7. Compared with Existing Methods

To demonstrate the reliability advantage of the proposed faulty feeder detection method, we compare it with three methods introduced in [3,18,19]. Figure 12 shows the high-frequency components of transient zero-sequence currents during an SPG fault occurring at 10% of F_4 with a fault inception angle of 90°, a fault resistance of 2000 Ω, and an SNR of 20 dB. In Figure 12, the difference in the first half-wave waveform between the faulty feeder and the healthy feeders is minimal. Consequently, detecting the faulty feeder based on the transient energy and waveform similarity of the high-frequency components of transient zero-sequence currents is challenging. Therefore, the faulty feeder detection method presented in [3] is ineffective under these conditions. Figure 13 illustrates the low-frequency components of zero-sequence currents during an SPG fault at 10% of F_4 with a fault inception angle of 90°, a fault resistance of 3000 Ω, and an SNR of 5 dB. In Figure 13, the faulty feeder F_4 exhibits the same polarity at the extreme values as the healthy feeders F_1, F_2, and F_3. Thus, the faulty feeder detection method proposed in [18] fails in this scenario. Table 6 summarizes the AR, FPR, and FNR of the faulty feeder detection methods proposed in this paper, as well as those in [3,18,19], based on the fault scenarios described in Section 4.4. As shown in Table 6, the proposed method achieves higher detection accuracy due to its ability to extract more effective fault characteristics.

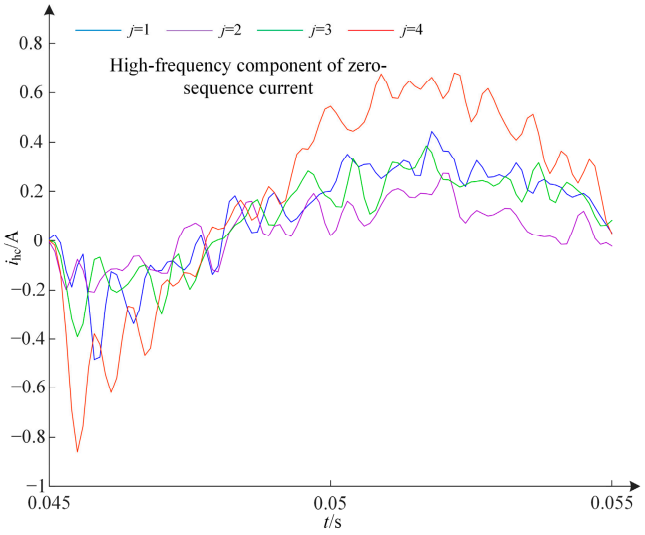


Figure 12. High-frequency components of transient zero-sequence currents.

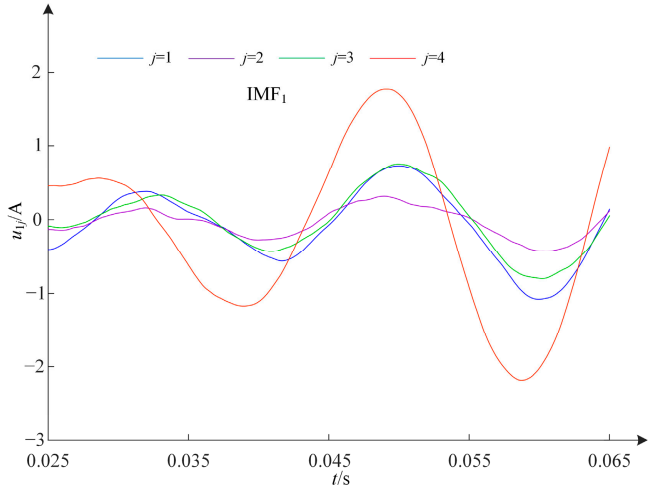


Figure 13. Low-frequency IMF1 of transient zero-sequence currents.

Table 6. Comparison of the faulty feeder detection accuracy of the proposed method with existing methods.

Fault Criterion	SNR	FPR	FNR	AR
Paper [3]	20	23.5%	8.8%	76.5%
Paper [3]	10	35.3%	17.6%	64.7%
Paper [3]	5	47.0%	23.5%	53.0%
Paper [18]	20	11.8%	2.9%	88.2%
Paper [18]	10	23.5%	5.9%	76.5%
Paper [18]	5	35.3%	14.7%	64.7%
Paper [19]	20	23.5%	23.5%	76.5%
Paper [19]	10	29.4%	26.5%	70.6%
Paper [19]	5	35.3%	32.4%	64.7%
This paper	20	0%	0%	100%
This paper	10	2.2%	2.2%	97.8%
This paper	5	5.9%	5.9%	94.1%

4.8. Field Test

To verify the feasibility of the proposed faulty feeder detection method for field applications, 20 sets of field data for SPG in a distribution network with 5 feeders are used for validation, and all results are accurate. At a substation in China with five feeders connected to a bus, the transient zero-sequence currents of each feeder during an SPG fault on feeder 4 are shown in Figure 14. The modal components IMF_1, IMF_2, and IMF_3 obtained by VMD are shown in Figure 14. As illustrated, compared to the other healthy feeders, the fault characteristics in IMF1 and IMF2 of feeder 4 are clearly distinguishable. The signals reconstructed according to Equation (7) are shown in Figure 15. The faulty feeder detection results, summarized in Table 7, are all correct. Therefore, the proposed faulty feeder detection method is suitable for application in actual distribution networks.

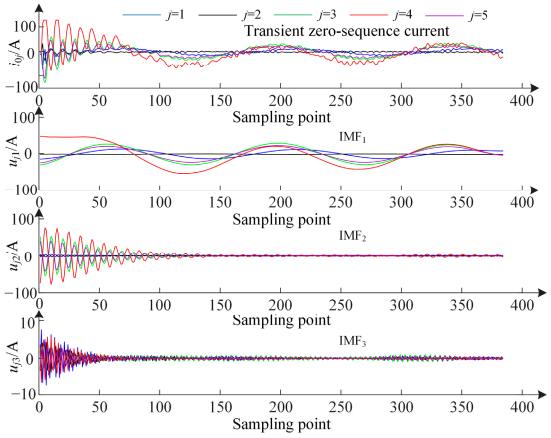


Figure 14. Transient zero-sequence currents of field data and IMFs.

Table 7. Faulty feeder detection result of field data.

E_j	ρ_j	η_j	Results
3190, 220, 50,610, 139,180, 30,440	0.9781, −0.6678, 0.9781	0.3727, −0.2545, 0.3727	Feeder 4

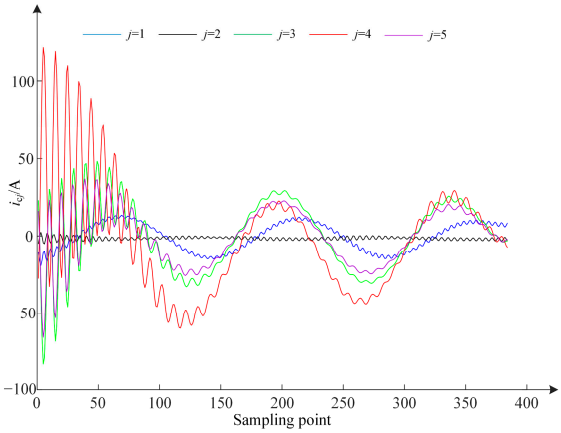


Figure 15. Reconstruction signals of field data.

5. Conclusions

In this study, we propose a faulty feeder detection method based on multiple transient characteristics fusion for resonant grounding systems. The main conclusions are as follows:

- There are significant differences in both the amplitude and polarity of the low-frequency and high-frequency components of the transient zero-sequence current between the faulty feeder and the healthy feeder at the initial fault instant. Additionally, the fault characteristics of the fundamental components within the low-frequency components are also distinctive. Therefore, the low-frequency and high-frequency components extracted from transient zero-sequence currents can be effectively used to detect faulty feeders.
- The fault characteristics of the signal, reconstructed from the low-frequency and high-frequency components of the transient zero-sequence current extracted through VMD, are clearly evident. By integrating the transient energy and waveform similarity of this reconstructed signal for faulty feeder detection, the method achieves high accuracy in identifying faulty feeders.
- Through numerous simulations and field data tests, it has been demonstrated that the accuracy of the proposed faulty feeder detection method remains unaffected by fault resistance, inception angle, fault location, or noise. Compared to two existing faulty feeder detection methods, the proposed method exhibits superior accuracy and adaptability in detecting faulty feeders.

The number of modes K and penalty factors α in VMD are fixed in this paper, which leads to incorrect detection of faulty feeders under varying fault scenarios. Developing methods to adaptively select VMD parameters will be the focus of our future research. Additionally, as distribution network structures become increasingly complex, the probability of multiple faults occurring in distribution networks continues to rise. The complex characteristics of multiple faults make detecting the faulty feeder particularly challenging. Therefore, effectively extracting features under multiple faults to accurately identify the faulty feeder will be a key focus of future research.

Author Contributions: Conceptualization, R.M.; Methodology, R.M.; Software, R.M.; Validation, R.M.; Formal analysis, R.M. and Q.P.; Investigation, R.M.; Resources, R.M.; Data curation, R.M.; Writing—original draft, R.M.; Writing—review and editing, Q.P.; Visualization, R.M.; Supervision, Q.P.; Project administration, R.M.; Funding acquisition, R.M. All authors have read and agreed to the published version of the manuscript.

Funding: This research was funded by the National College Students' Innovative Entrepreneurial Training Plan Program of China (Grant No. 202510429030).

Data Availability Statement: The original contributions presented in this study are included in the article. Further inquiries can be directed to the corresponding author.

Conflicts of Interest: The authors declare no conflicts of interest.

References

1. Wei, M.; Shi, F.; Zhang, H.; Chen, W. Wideband Synchronous Measurement-Based Detection and Location of High Impedance Fault for Resonant Distribution Systems with Integration of DERs. *IEEE Trans. Smart Grid* **2023**, *14*, 1117–1134. [CrossRef]
2. Wang, X.; Zhang, H.; Shi, F.; Wu, Q.; Terzija, V.; Xie, W.; Fang, C. Location of Single Phase to Ground Faults in Distribution Networks Based on Synchronous Transients Energy Analysis. *IEEE Trans. Smart Grid* **2020**, *11*, 774–785. [CrossRef]
3. Wei, X.; Wang, X.; Gao, J.; Yang, D.; Wei, K.; Guo, L. Faulty Feeder Detection for Single-Phase-to-Ground Fault in Distribution Networks Based on Transient Energy and Cosine Similarity. *IEEE Trans. Power Deliv.* **2022**, *37*, 3968–3978. [CrossRef]
4. Yuan, J.; Xing, L.; Xue, M.; Chen, Q.; Hu, B.; Chen, X.; Liu, J.; Jiao, Z. A Highly Reliable Image-Recognition-Based Intelligent Fault Detection Method for Feeders Using Fully Convolutional Generative Adversarial Network. *IEEE Trans. Smart Grid* **2025**, *16*, 2278–2291. [CrossRef]
5. Wei, X.; Yang, D.; Wang, X.; Wang, B.; Gao, J.; Wei, K. Faulty Feeder Detection Based on Fundamental Component Shift and Multiple-Transient-Feature Fusion in Distribution Networks. *IEEE Trans. Smart Grid* **2021**, *12*, 1699–1711. [CrossRef]
6. Yuan, J.; Jiao, Z. Faulty-Feeder Detection for Single Phase-to-Ground Faults in Distribution Networks Based on Waveform Encoding and Waveform Segmentation. *IEEE Trans. Smart Grid* **2023**, *14*, 4100–4115. [CrossRef]
7. Liu, P.; Du, S.; Sun, K.; Zhu, J.; Xie, D.; Liu, Y. Single-Line-to-Ground Fault Feeder Selection Considering Device Polarity Reverse Installation in Resonant Grounding System. *IEEE Trans. Power Deliv.* **2021**, *36*, 2204–2212. [CrossRef]
8. Milioudis, A.H.; Andreou, G.T.; Labridis, D.P. Detection and Location of High Impedance Faults in Multiconductor Overhead Distribution Lines Using Power Line Communication Devices. *IEEE Trans. Smart Grid* **2021**, *12*, 894–902. [CrossRef]
9. Lin, Y.-H.; Liu, C.-W.; Chen, C.-S. A new PMU-Based Fault Detection/Location Technique for Transmission Lines with Consideration of Arcing Fault Discrimination-Part I: Theory and Algorithms. *IEEE Trans. Power Deliv.* **2004**, *19*, 1587–1593. [CrossRef]
10. Wang, B.; Geng, J.; Dong, X. High Impedance Fault Detection Based on Nonlinear Voltage-Current Characteristic Profile Identification. *IEEE Trans. Smart Grid* **2018**, *9*, 3783–3791. [CrossRef]
11. Wang, X.; Wei, X.; Yang, D.; Song, G.; Gao, J.; Wei, Y.; Zeng, Z.; Peng, W. Fault Feeder Detection Method Utilized Steady State and Transient Components Based on FFT Backstepping in Distribution Networks. *Int. J. Elect. Power Energy Syst.* **2020**, *114*, 105391.
12. Costa, F.B. Fault-Induced Transient Detection Based on Real-Time Analysis of the Wavelet Coefficient Energy. *IEEE Trans. Power Deliv.* **2014**, *29*, 140–153. [CrossRef]
13. Gao, J.; Wang, X.; Wang, X.; Yang, A.; Yuan, H.; Wei, X. A High-Impedance Fault Detection Method for Distribution Systems Based on Empirical Wavelet Transform and Differential Faulty Energy. *IEEE Trans. Smart Grid* **2022**, *13*, 900–912. [CrossRef]
14. Guo, Z.; Yao, J.; Tan, Z. Hilbert-Huang Transform-Based Transient Busbar Protection Algorithm. *IET Gener. Transm. Distrib.* **2015**, *9*, 2032–2039. [CrossRef]
15. Wang, X.; Gao, J.; Wei, X.; Zeng, Z.; Wei, Y.; Kheshti, M. Single Line to Ground Fault Detection in a Non-Effectively Grounded Distribution Network. *IEEE Trans. Power Deliv.* **2018**, *33*, 3173–3186. [CrossRef]
16. Tang, T.; Zeng, X.; Huang, C.; Li, Z. Faulty Feeder Detection Based on the Composite Factors in Resonant Grounding Distribution System. *Electric Power Syst. Res.* **2020**, *189*, 106578. [CrossRef]
17. Wang, X.; Gao, J.; Wei, X.; Song, G.; Wu, L.; Liu, J.; Zeng, Z.; Kheshti, M. High Impedance Fault Detection Method Based on Variational Mode Decomposition and Teager-Kaiser Energy Operators for Distribution Network. *IEEE Trans. Smart Grid* **2019**, *10*, 6041–6054. [CrossRef]
18. Wang, X.; Gao, J.; Wei, X.; Guo, L.; Song, G.; Wang, P. Faulty Feeder Detection Under High Impedance Faults for Resonant Grounding Distribution Systems. *IEEE Trans. Smart Grid* **2023**, *14*, 1880–1895. [CrossRef]
19. Yin, Z.; Wei, Z.; Sun, G.; Chen, S.; Zang, H. Unified Faulty Feeder Detection Criteria and High-Speed Protection Scheme for High Impedance Faults in Resonant Grounding MV Networks. *IEEE Trans. Smart Grid* **2025**, *16*, 3653–3665. [CrossRef]
20. Xue, Y.; Li, J.; Xu, B. Transient Equivalent Circuit and Transient Analysis of Single-Phase Earth Fault in Arc Suppression Coil Grounded System. *Proc. CESS* **2015**, *35*, 5703–5714.
21. Xue, Y.; Chen, X.; Song, H.; Xu, B. Resonance Analysis and Faulty Feeder Identification of High-Impedance Faults in a Resonant Grounding System. *IEEE Trans. Power Deliv.* **2017**, *32*, 1545–1555. [CrossRef]
22. Guo, M.; Zeng, X.; Chen, D.; Yang, N. Deep-Learning-Based Earth Fault Detection Using Continuous Wavelet Transform and Convolutional Neural Network in Resonant Grounding Distribution Systems. *IEEE Sens. J.* **2018**, *18*, 1291–1300. [CrossRef]
23. Alenezi, M.; Anayi, F.; Packianather, M.; Shouran, M. A Hybrid Machine Learning Framework for Early Fault Detection in Power Transformers Using PSO and DMO Algorithms. *Energies* **2025**, *18*, 2024. [CrossRef]

24. Moloi, K.; Davidson, I. High Impedance Fault Detection Protection Scheme for Power Distribution Systems. *Mathematics* **2022**, *10*, 4298. [CrossRef]
25. Yu, X.; Cao, J.; Fan, Z.; Xu, M.; Xiao, L. Faulty Feeder Identification in Resonant Grounding Distribution Networks Based on Deep Learning and Transfer Learning. *CSEE J. Power Energy Syst.* **2023**, *9*, 2168–2178.
26. Wang, X.; Jiang, H.; Dong, Y.; Mu, M. Spatial-channel collaborative multi-scale graph interaction deep transfer learning for unsupervised rotating machinery fault diagnosis. *Eng. Appl. Artif. Intell.* **2026**, *176*, 114691. [CrossRef]
27. Wu, Z.; Jiang, H.; Wang, X.; Zhu, H. Knowledge Correlation Graph-Guided Multi-Source Interaction Domain Adaptation Network for Rotating Machinery Fault Diagnosis. *ISA Trans.* **2023**, *142*, 663–682. [CrossRef]
28. Darvishi, H.; Ciuonzo, D.; Rossi, P.S. Deep Recurrent Graph Convolutional Architecture for Sensor Fault Detection, Isolation, and Accommodation in Digital Twins. *IEEE Sens. J.* **2023**, *23*, 29877–29891. [CrossRef]
29. Cartocci, N.; Napolitano, M.R.; Crocetti, F.; Costante, G.; Valigi, P.; Fravolini, M.L. Data-Driven Fault Diagnosis Techniques: Non-Linear Directional Residual vs. Machine-Learning-Based Methods. *Sensors* **2022**, *22*, 2635. [CrossRef]
30. Dragomiretskiy, K.; Zosso, D. Variational Mode Decomposition. *IEEE Trans. Signal Process.* **2014**, *62*, 531–544. [CrossRef]
31. Mo, Y.; Lyu, Y.; Wang, H.; Zhao, W.; Chen, H. Improved VMD with hybrid grey wolf optimization for bearing signal fault analysis. *Measurement* **2026**, *264*, 120312. [CrossRef]

Disclaimer/Publisher's Note: The statements, opinions and data contained in all publications are solely those of the individual author(s) and contributor(s) and not of MDPI and/or the editor(s). MDPI and/or the editor(s) disclaim responsibility for any injury to people or property resulting from any ideas, methods, instructions or products referred to in the content.